Pharm Res (2012) 29:1087–1097
DOI 10.1007/s11095-011-0653-9

RESEARCH PAPER

Preparation, Characterization of 2-Deoxy-D-Glucose Functionalized Dimercaptosuccinic Acid-Coated Maghemite Nanoparticles for Targeting Tumor Cells

Fei Xiong • Zi-yi Zhu • Chen Xiong • Xiao-qing Hua • Xiu-hong Shan • Yu Zhang • Ning Gu

Received: 20 September 2011 / Accepted: 6 December 2011 / Published online: 16 December 2011

ABSTRACT

Purpose To report a modified preparation and to systematically study the structure, magnetic and other properties of γ-Fe_2O_3-DMSA-DG NPs (2-deoxy-D-glucose (2-DG) conjugated meso-2,3-dimercaptosuccinic acid coated γ-Fe_2O_3 nanoparticles) and test its ability to improve Hela tumor cells targeting *in vitro* compared to the γ-Fe_2O_3-DMSA NPs.

Methods The conjugation of 2-DG on the surface of γ-Fe_2O_3-DMSA NPs was performed by esterification reaction and characterized. Acute toxicity was evaluated using MTT assay. Cellular uptake was investigated by Prussian blue staining and UV colorimetric assay.

Results DG was successfully functionalized onto the surface of γ-Fe_2O_3-DMSA NPs; binding efficiency was ~60%. The mean diameter of single core of γ-Fe_2O_3-DMSA-DG NPs was 10 nm. Particle size and polydispersity index of its aggregates were 156.2 nm and 0.162, respectively. 2-DG-conjugated nanoparticles caused little cytotoxic effects on Hela cells at the concentration range of 0–600 μg/mL. When 2-DG-conjuated and non-conjugated nanoparticles were incubated with Hela cells for 4, 8 and 12 h, the 2-DG-conjugated nanoparticle showed significant amount of uptake in cells compared to their non-targeted counterparts.

Conclusion γ-Fe_2O_3-DMSA-DG NPs could be developed as a tumor-targeted probe for cervical cancer imaging and therapy.

KEY WORDS 2-deoxy-D-glucose · hela cells · iron oxide nanoparticles

ABBREVIATIONS

2-DG	2-deoxy-D-glucose
γ-Fe_2O_3-DMSA NPs	meso-2,3-dimercaptosuccinic acid coated γ-Fe_2O_3 nanoparticles
γ-Fe_2O_3-DMSA-DG NPs	2-deoxy-D-glucose (2-DG) conjugated meso-2,3-dimercaptosuccinic acid coated γ-Fe_2O_3 nanoparticles
DMSA	meso-2,3-dimercaptosuccinic acid
EDC	1-Ethyl-(3-3-dimethylaminopropyl) carbodiimide hydrochloride
FCS	fetal calf serum
FTIR	fourier transform infrared
GLUT	glucose transporter
MRI	magnetic resonance imaging
Ms	saturation magnetization value
NHS	N-hydroxysuccinimide
SPIO NPs	superparamagnetic iron oxide nanoparticles
TEM	transmission electron microscopy
TGA	thermal gravimetric analysis
VSM	vibrating sample magnetometer

F. Xiong • Z.-y. Zhu • X.-q. Hua • Y. Zhang • N. Gu (✉)
State Key Laboratory of Bioelectronics
Jiangsu Laboratory for Biomaterials and Devices
School of Biological Science & Medical Engineering
Southeast University
2 Sipailou
Nanjing, China
e-mail: guning@seu.edu.cn

C. Xiong
Department of Pharmacology, School of Basic Medicine
Hebei Medical University
Shijiazhuang, China

X.-h. Shan
Department of Radiology
The Affiliated Renmin Hospital
Jiangsu University
Zhenjiang, China

INTRODUCTION

Tumor cells have acquired metabolic abilities to survive under unfavorable microenvironment conditions thus developing a more aggressive phenotype. Increased glucose utilization is one of the most characteristic and early-recognized biochemical markers of the transformed phenotype (1). Therefore, some researchers have proposed the glucose transporter (GLUT) as an important diagnostic and therapeutic target to modulate the accelerated tumor growth (2,3). GLUT activity in mammalian cells has been monitored by radiolabeled tracers such as [^{14}C] 2-deoxy-D-glucose, [^{18}F] fluoro-2-deoxy-D-glucose, and [^{14}C] or [^{3}H]3-*O*-methyl-D-glucose (4–7). [^{18}F] fluoro-2-deoxy-D -glucose (^{18}F-FDG) is the most common radiotracer of increased glucose metabolism to visualize tumor activity and location with positron emission tomography (PET) in the clinical setting. The method is sensitive and quantitative (4,8). For many high throughput preclinical studies, however, ^{18}F-FDG is impractical due to the short half-life of the isotope. Therefore, alternatives to 2-deoxy-D-glucose (2-DG) labeled imaging agents would be valuable. Among the imaging modalities, magnetic resonance imaging (MRI) is a powerful medical diagnostic imaging technique for soft tissue imaging (9). Other advantages of MRI include the use of nonionizing radiation, high sensitivity and higher specificity, multiplanar imaging capability, and high anatomical resolution. Superparamagnetic iron oxide nanoparticles (SPIO NPs, Fe_3O_4 or γ-Fe_2O_3) are one of the most adopted magnetic nanoprobes for T_2 weighted MRI studies. In addition, especially in the last decade, the field of biomedicine witnessed an explosion of interest in the use of magnetic nanomaterial in magnetic cell labeling and sorting, effective treatment of some diseases, such as anti-tumor drug and gene delivery and guided hyperthermia therapy (10–18).

For develop a novel targeted magnetic nanoprobes based on higher glucose consumption of tumor cell, we reported preparation, transmission electron microscopy (TEM) and infrared spectroscopy (IR) characterization of a novel 2-deoxy-D-glucose (2-DG) conjugated SPIO NPs, abbreviated as γ-Fe_2O_3-DMSA-DG NPs, for targeting MDA-MB-231 human breast cancer cells in previous paper (19). These γ-Fe_2O_3-DMSA-DG NPs were synthesized by conjugating amino groups of 2-DG to surface carboxyl groups of meso-2, 3-dimercaptosuccinic acid (DMSA) coated γ-Fe_2O_3 NPs (γ-Fe_2O_3-DMSA NPs). In this report, our goal was to report a modified preparation and systematically study the structure, magnetic and other properties of γ-Fe_2O_3-DMSA-DG NPs and test its ability to improve the Human cervical cancer cells (Hela) tumor cells target *in vitro* as compared the γ-Fe_2O_3-DMSA NPs. This lays down the groundwork for us to research and develop a multifunctional tumor-targeted SPIO NPs for follow-up applications in the field of magnetic cell separation, MRI, hyperthermia, drug delivery and gene therapy.

MATERIALS AND METHODS

Materials

meso-2, 3-dimercaptosuccinic acid (DMSA) was purchased from Shanghai Beihe Chemicals Co. Ltd, China. D-Glucosamine (2-amino-2-deoxy-D-glucose) hydrochloride (ADG·HCl) was purchased from Alfa Aesar GmbH & Co. KG. 1-Ethyl-(3-3-dimethylaminopropyl) carbodiimide hydrochloride (EDC) and N-hydroxysuccinimide (NHS) were purchased from Pierce Chemical Co. Human cervical cancer cells (Hela) were perchased from Shanghai Cellular Institute of China Scientific Academy. RPMI 1640 medium (containing 10% fetal calf serum, 100 μg/mL penicillin, and 100 μg/mL streptomycin), glucose-free RPMI 1640 medium and fetal calf serum were purchased from BoooCle Bio-Tech Co.,Ltd. GLUT1 antibody was purchased from Shengyan Biomedicals (Shanghai) Co., Ltd. The other chemicals were analytical grade reagents and purchased from Shanghai Chemical Reagent Corporation, China. All chemicals were used as received. Double distilled water was used for all the experiments. Dialysis tubing (MW: 8000–10000) was purchased from Nanjing Genetime Biotechnology Co., LTD.

Synthesis of γ-Fe_2O_3-DMSA-DG NPs

γ-Fe_2O_3 NPs were synthesized by chemical co-precipitation and subsequently stabilized with DMSA as described earlier (20). Briefly, a 200 mL mixed solution of $FeCl_3{\cdot}6H_2O$ (0.01 M) and $FeSO_4{\cdot}7H_2O$ (0.006 M) at pH 1.7 was prepared under a stream of N_2 protecting. Then, aqueous ammonia solution (1.5 M) was dropped into it with violently stirring until the pH of the solution was raised to 9. The balanced equation was as follows:

$$Fe^{2+} + 2Fe^{3+} + 8OH^- \rightarrow Fe_3O_4 + 4H_2O$$

The obtained magnetite was washed immediately with water for 5 times and ethanol for 2 times by magnetic separation. Then, the Fe_3O_4 NPs were dispersed in water with a mass concentration of 3 mg/mL and its pH was adjusted to 3.0 using 0.1 M HCl. Then theses Fe_3O_4 NPs were oxidized into reddish-brown γ-Fe_2O_3 NPs using air for 1 h at about 95–100°C. Subsequently, the γ-Fe_2O_3 NPs

were coated with DMSA according to the process described elsewhere (21,22). Finally, the products were washed repeatedly with water and enriched with the help of a magnet.

The immobilization of 2-DG on γ-Fe_2O_3-DMSA NPs via esterification reaction was according to the process reported with modification (19). Surface activation was performed by exposing the acid surface to EDC (0.5 mM) and NHS (2.5 mM). For improving the conjugation efficiency, EDC (0.5 mM) and NHS (2.5 mM) were added for three times with 1 mL per time into 10 mL γ-Fe_2O_3-DMSA NPs (1 mM). The mixed solution was left at room temperature for 30 min. Add 10 mL of ADG·HCl (final concentration: 2 mg/mL) to 20 mL solution above. React for 2 h at room temperature. Purify by dialysis overnight against water (dialysis tubing, MW: 8000–10000).

Characterization

TEM studies and electron diffraction (ED) were carried out using a JEM-2000EX (Jeol, Japan). A drop of particles suspension in water was placed on a carbon-coated copper grid (300 mesh), followed by drying the sample at room temperature before it is attached to the sample holder on the microscope. The structure of the crystal was determined from its ED.

The functional groups present in the powder samples of ADG·HCl, DMSA, γ-Fe_2O_3-DMSA NPs and γ-Fe_2O_3-DMSA-DG NPs were identified by fourier transform infrared (FTIR) spectroscopy. FTIR spectra were recorded on a Nicolet Nexus 870 FTIR spectrometer (Nicolet, USA) and 1% of the powder samples were mixed and ground with 99% KBr. Discs of 10 mm diameter were prepared by pressing the powder mixture at a load of 10 tons under vacuum for 2 min and the spectrum was taken in the range of 4000-400 cm^{-1} with a resolution of 2 cm^{-1}at room temperature.

The elemental analysis and 2-DG loading on γ-Fe_2O_3-DMSA NPs were measured by energy dispersive X-ray spectroscopy (SEM/EDS, EDAX, PV9100).

The thermal behaviour of the powders was studied by thermal gravimetric analysis (TGA) using a Perkin-Elmer TGA 7 Thermogravimetric Analyzer in synthetic N_2 atmosphere up to 700°C.

Magnetic measurements were carried out with a Lakeshore 7470 vibrating sample magnetometer (VSM) (Lakeshore, 7407 VSM system). The samples were dried by heating at 80°C.

The hydrodynamic diameter and size distribution of the particles were determined at 25°C by photon correlation spectroscopy (PCS) instrument (Malvern Zetasizer 3000, Malvern Instruments Co.). The zeta potential was obtained by measuring the electrophoretic mobility (Malvern Zetasizer 3000, Malvern Instruments Co.). All samples were diluted 100 times by water.

Cell Culture, Cytotoxicity and Uptake Experiments

Hela cells were cultured in RPMI 1640 medium containing 10% fetal calf serum (FCS), 100 μg/mL penicillin, and 100 μg/mL streptomycin. For control experiments, medium having no particle was used. The cells were incubated at 37°C in 5% CO_2 atmosphere and medium was replaced every third day.

The cytotoxicity of γ-Fe_2O_3-DMSA-DG NPs was evaluated by using a 3-[4,5-dimethylthiazol-2-yl]-2,5-diphenyl tetrazolium bromide (MTT) assay. The Hela cells were grown in 96-well plates at 5×10^4 cells per well at 37°C in 5% CO_2 atmosphere for 24 h. The culture medium was replaced with 100 mL of medium containing 0–600 μg/mL of nanoparticles. The cytotoxicity was evaluated by determining the viability of Hela cells. After incubation for 24 h, the medium was removed and rinsed once with medium, MTT dye solution (5 mg/mL) was added to each well. After 4 h of incubation at 37°C, the medium was removed and Formazan crystals were dissolved in 200 μL dimethylsulphoxide (DMSO) and quantified by measuring the absorbance of the solution by a microplate reader (Ultra Microplate Reader EL×808 IU, Bio-RAD) at 570 nm. The viability was calculated as the percentage of control (cells receiving no treatment).

In the cell-uptake experiments, cells were washed with PBS and medium was changed to glucose-free RPMI 1640. The dilutions of γ-Fe_2O_3-DMSA NPs and γ-Fe_2O_3-DMSA-DG NPs were added for the concentration, time and temperature indicated. For Prussian blue staining, which indicates the presence of iron, one part of the cells was fixed with 2.5% glutaraldehyde at 4°C for 1 h, washed, and incubated for 30 min with 2% potassium ferric-ferrocyanide in 3.7% hydrochloric acid. Cells were washed again and evaluated for iron staining using light microscopy (Axioplan Imaging II, Zeiss, Germany).

Cellular uptake of γ-Fe_2O_3-DMSA NPs and γ-Fe_2O_3-DMSA-DG NPs was determined by measuring the Fe concentration. The cell layer was dissolved in 30% v/v HCl at 60°C for 2 h. A total of 1.0 mg of potassic persulphate was then added to oxidize the ferrous ions present in the above solution to ferric ions. Then 1.0 mL of 0.1 M solution of potassium thiocyanate was added to this solution to form the iron-thiocyante complex. 150 μl of the mixture was transferred to a 96-well plate and the absorbance was read after 10 min at 480 nm using a microplate reader (Model 680, Bio-RAD) (23). A standard curve using the differently

$FeCl_3 \cdot 6H_2O$ solution was recorded in the same conditions to quantify the amount of cell-bound iron. Each experiment was repeated in triplicate wells at least three times. Means and standard deviations were calculated.

To determine the competitive effect and specificity of glucose, Hela cells were inclubated at 37°C with 2 μg/mL anti-GLUT1 antibody before γ-Fe_2O_3-DMSA NPs or γ-Fe_2O_3-DMSA-DG NPs were added. NPs were added to a final concentration of 100 μg/mL and cells were incubated at 37°C for another 2 h. SPIO NPs in cells were stained with Prussian blue as described above.

MRI

To evaluate the potential of SPIO NPs in clinical MR imaging, labeled Hela cells after incubation 2 h were trypsinized, centrifuged, counted, and resuspended in 2% agarose in Eppendorf tubes. MRI was performed at 1.5 T (Siemens Ananto1.5 T System) for T_2 weighted imaging (T_2WI) by using a fast spin-echo sequence (repetition time/echo time (TR/TE), 5500 ms/100 ms; field of view (FOV), 50 mm× 50 mm; slice thickness, 3 mm; matrix, 256×256) and a16-echo sequence (TR/TE, 3000 ms/22 ms, 44 ms, 66 ms, 88 ms,110 ms,…… 352 ms; FOV, 50 mm×50 mm; slice thickness, 3 mm; matrix, 256×256) at room temperature. The signal intensities of the nonlabeled and γ-Fe_2O_3-DMSA NPs or γ-Fe_2O_3-DMSA-DG NPs–labeled cells were determined from a circular 10-mm^2 region of interest (ROI).

RESULTS

Synthesis of γ-Fe_2O_3-DMSA-DG NPs

The γ-Fe_2O_3 NPs were synthesized by chemical coprecipitation and stable nanoparticles suspension was obtained via surface coating with DMSA. Over amount of $FeSO_4 \cdot 7H_2O$ was required in this reaction in order to prevent possible oxidation of Fe^{2+}. Then the pH of mixed solution was adjusted to 9 using aqueous ammonia solution in order to make sure black Fe_3O_4 was precipitated absolutely. There are two theories to explain the possible mechanism of binding of DMSA to SPIO NPs. One theory is strong coordinate bonds between Fe and S of DMSA were formed (24). The other theory is coordinate bonds between Fe and COOH of DMSA were formed (25). For conjugating 2-DG to the surface of nanoparticles, surface acylamidation reaction was introduced in this paper outlined in Fig. 1. This surface reaction allows the formation of carboxylic acid groups on the γ-Fe_2O_3-DMSA NPs surface that, once activated with EDC, are competent for reacting with primary amino groups on the 2-DG.

Characterization

The TEM images of γ-Fe_2O_3-DMSA NPs and γ-Fe_2O_3-DMSA-DG NPs are shown in Fig. 2, which shows that most of the particles are quasi-spherical and the average diameter of single core of NPs are 10 nm. The particle aggregates are well dispersed in water in both Fig. 2 (a) and (b). Under conditions of room temperature and air-induced oxidation, γ-form of Fe_2O_3 core was the only possible crystal structure produced. Other crystal structure, for example, α-Fe_2O_3 NPs were not produced because the phase transition of γ-Fe_2O_3 to α-Fe_2O_3 occurred at the temperature range of 580–608°C in the dependence on the particle size (26). ED measurements were also performed to confirm the crystal form of γ-Fe_2O_3-DMSA-DG NPs prepared. The result is shown in Fig. 2(c). Each diffraction ring coincides with the diffraction ring of γ-Fe_2O_3 reported (27,28).

Qualitative characterization of γ- Fe_2O_3-DMSA-DG NPs was achieved by SEM/EDS and FTIR. Figure 3a

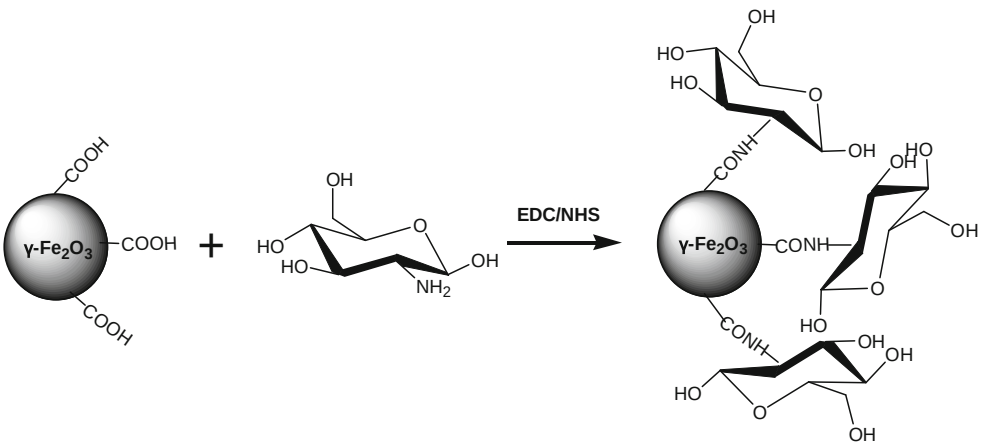

Fig. 1 The synthetic scheme of γ-Fe_2O_3-DMSA-DG NPs.

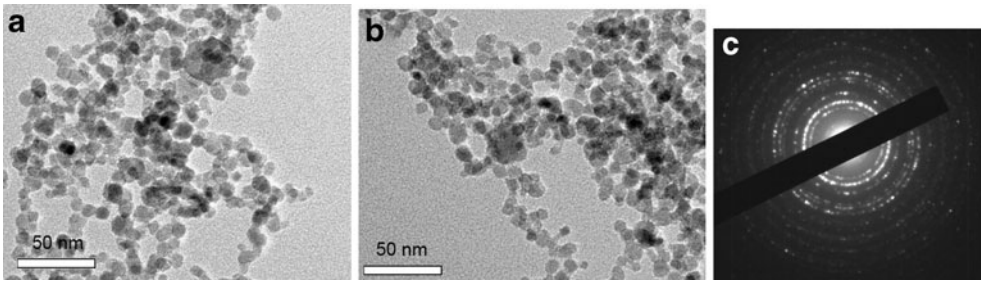

Fig. 2 TEM images of γ-Fe_2O_3-DMSA NPs (**a**) and γ-Fe_2O_3-DMSA-DG NPs (**b**); ED patterns of γ-Fe_2O_3-DMSA-DG NPs (**c**).

demonstrates that DG are successfully functionalized onto the surface of γ-Fe_2O_3-DMSA NPs as evidenced in the FTIR spectra of γ-Fe_2O_3-DMSA NPs and γ- Fe_2O_3-DMSA-DG NPs. The FTIR data of ADG·HCl, DMSA, γ-Fe_2O_3-DMSA NPs and γ- Fe_2O_3-DMSA-DG NPs are listed in Table I. The band at 1088 and 1052 cm^{-1} in the FTIR curve of γ- Fe_2O_3-DMSA-DG NPs corresponded to C-N and C-O stretching vibration of 2-DG, respectively. Thus, IR results confirm the successful surface 2-DG functionlization of γ-Fe_2O_3-DMSA NPs.

Figure 3b shows a typical SEM/EDS elemental analysis of γ-Fe_2O_3-DMSA NPs and γ- Fe_2O_3-DMSA-DG NPs. From the peak area of N, the atomic ratio of N was increased from 0 to 4.97% after conjugation of 2-DG on the surface of γ- Fe_2O_3-DMSA NPs. This also indicated 2-DG was successfully functionalized onto the surface of γ-Fe_2O_3-DMSA NPs

TGA has been performed to confirm the coating formation and estimate the binding efficiency of DMSA and 2-DG on the surface of γ-Fe_2O_3 NPs for quantitative characterization of γ-Fe_2O_3-DMSA-DG NPs. Fig. 4 shows the weight loss for γ- Fe_2O_3-DMSA NPs and γ-Fe_2O_3-DMSA-DG NPs. A slight weight loss (8.19% in Fig. 4(a), 15.69% in Fig. 4(b)) is observed up to 250°C in both curves, probably due to adsorbed water, while a significant weight loss takes place between 250 and 600°C. The weight loss for γ-Fe_2O_3-DMSA NPs, attributed to decomposition of DMSA, is 4.95%, corresponding to the molar ratio between the Fe and DMSA (100:2.5) or the number ratio between Fe_2O_3 NPs and DMSA (1:516). The calculation was as follows:

the number ratio between Fe_2O_3 NPs and DMSA in $\gamma - Fe_2O_3 -$ DMSA NPs system

$$= 1 : 516 = \frac{3(1 - W_{l1}\% - W_{l2}\%)}{4\rho\pi R^3 N_A} : \frac{W_{l1}\%}{M_1}$$

where W_{l1}% is weight loss percentage of DMSA of γ-Fe_2O_3-DMSA NPs, W_{l2}% is weight loss percentage of water in γ-Fe_2O_3-DMSA NPs sample, ρ is the density of Fe_2O_3, R is the radius of Fe_2O_3 nanoparticle, M_1 is molecular weight of DMSA, N_A is Avogadro's number.

The weight loss for γ-Fe_2O_3-DMSA-DG NPs between 250 and 600°C is increased to 9.31%, mainly due to the decomposition of DMSA and ADG.. Assuming the weight for γ-Fe_2O_3 NPs in the Fig. 4 (a) and (b) is 86.86% and 75.23% respectively, and according the molecular weight of DMSA and ADG is 182.2 and 179.1 respectively, we could calculate the molar ratio between DMSA and ADG (1 : 1.2) in the γ-Fe_2O_3-DMSA-DG NPs system. The calculation was as follows:

the molar ratio between DMSA and ADG in the $\gamma - Fe_2O_3 -$ DMSA $-$ DG NPs system

$$= 1 : 1.2 = \frac{\left[W_{l3}\% - \frac{(1-W_{l3}\%-W_{l4}\%)W_{l1}\%}{1-W_{l1}\%-W_{l2}\%}\right]}{M_2} : \frac{\frac{(1-W_{l3}\%-W_{l4}\%)W_{l1}\%}{1-W_{l1}\%-W_{l2}\%}}{M_1}$$

where W_{l3}% is weight loss percentage of DMSA and ADG of γ-Fe_2O_3-DMSA-DG NPs, W_{l4}% is weight loss percentage of water in γ-Fe_2O_3-DMSA-DG NPs sample, M_2 is molecular weight of ADG. Considering that DMSA is a compound with two carboxyl groups, the binding efficiency of 2-DG on the surface of γ- Fe_2O_3-DMSA NPs is about 60% (carboxyl group:2-DG=10:6).

The hysteresis loop of the as-synthesized magnetic NPs is shown in Fig. 5, which is measured at room temperature with a VSM. Magnetic measurements indicated superparamagnetic behavior at room temperature for both samples, as evidenced by zero coercivity and remanence on the magnetization loops. The saturation magnetization value (Ms) for γ- Fe_2O_3-DMSA NPs and γ- Fe_2O_3-DMSA-DG NPs was 48.95 and 49.67 emu/g, respectively. The Ms of both NPs was similar to the value reported previously (29,30) and enough to be used as MRI probe. It can be concluded there was no significant reduction of the Ms after conjugation reaction.

The dispersion in water of γ- Fe_2O_3-DMSA NPs and γ-Fe_2O_3-DMSA-DG NPs produced nanoparticle aggregates. PCS was applied to determine the average hydrodynamic diameter and polydispersity index of these aggregates. The

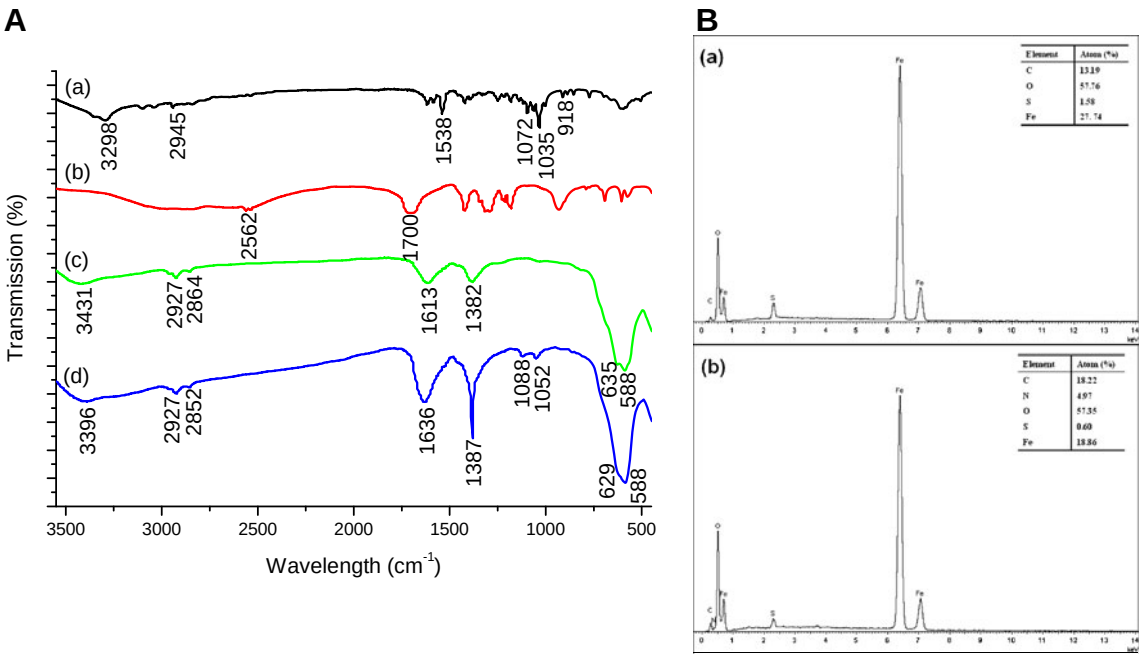

Fig. 3 Qualitative characterization of γ-Fe_2O_3-DMSA-DG NPs. (**A**) IR of ADG·HCl (**a**), DMSA (**b**), γ-Fe_2O_3-DMSA NPs (**c**) and γ-Fe_2O_3-DMSA-DG NPs (**d**); (**B**) SEM/EDS elemental analysis of γ-Fe_2O_3-DMSA NPs (**a**) and γ-Fe_2O_3-DMSA-DG NPs (**b**).

average hydrodynamic diameter (the mean diameter based upon the intensity of scattered light) of γ- Fe_2O_3-DMSA NPs and γ- Fe_2O_3-DMSA-DG NPs was 154.6±28.3 and 156.2±28.2 nm, respectively, which was the total diameter of aggregates and its aqueous layer thickness. The polydispersity index is a ratio that gives information about the homogeneity of the particle size distribution in a given system. In this paper, polydispersity index was applied to evaluate the monodisperse population of particle aggregates. The zeta potential of γ-Fe_2O_3-DMSA NPs and γ-Fe_2O_3-DMSA-DG NPs was (-21.76±0.80) and (-10.22±0.81) mV, respectively. This decrease in surface negative charge was due to the absence of some carboxyl groups on the surface of γ-Fe_2O_3-DMSA-DG NPs after conjugation of ADG to these carboxyl groups. The polydispersity index of γ- Fe_2O_3-DMSA NPs and γ- Fe_2O_3-DMSA-DG NPs was 0.146 and 0.162, respectively. Considering no significant difference of particle size and distribution between γ- Fe_2O_3-DMSA NPs and γ-Fe_2O_3-DMSA-DG NPs was detected, it suggested that no bigger aggregates generated during conjugation reaction.

Table I FTIR Data and Spectra Analysis of ADG·HCl, DMSA, γ- Fe_2O_3-DMSA NPs and γ-Fe_2O_3-DMSA-DG NPs

	ADG·HCl	DMSA	γ- Fe_2O_3-DMSA NPs	γ- Fe_2O_3-DMSA-DG NPs
O-H stretching vibration			3431(w)	3396(w)
N-H stretching vibration	3298(w)			
C-H asymmetric/symmetric stretching vibration	2945(w)		2927/2864(w)	2927/2852(w)
S-H stretching vibration		2562(w)		
C=O stretching vibration		1700(m)		
O-H bending vibration			1613(m)	1636(m)
N-H inplane bending vibration	1538(m)			
C-H scissoring vibration			1382(m)	1387(m)
C-N stretching vibration	1072(w)			1088(w)
C-O stretching vibration	1035(m)			1052(w)
N-H out-plane bending vibration	918(w)			
Fe-O lattice vibration (stretching/bending vibration)			635/588(s)	629/588(s)

s strong, *m* medium, *w* weak

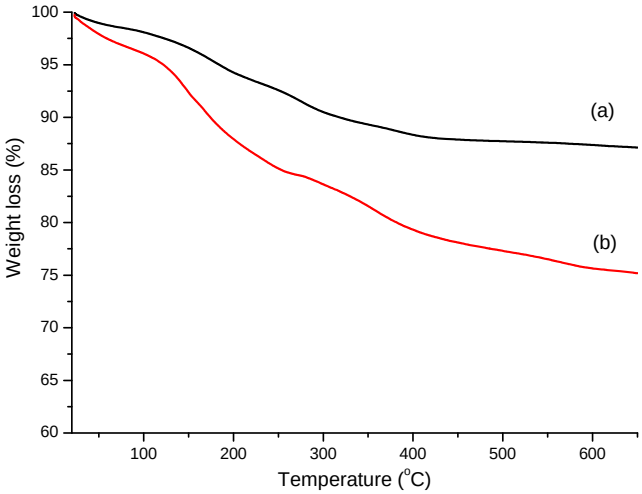

Fig. 4 TGA curves of γ-Fe_2O_3-DMSA NPs (a) and γ-Fe_2O_3-DMSA-DG NPs (b).

MTT Cytotoxicity Assay

To examine the acute toxicity of γ-Fe_2O_3-DMSA NPs and γ-Fe_2O_3-DMSA-DG NPs, the viability of Hela cells incubated with the nanoparticles at the concentration range of 0–600 μg/mL was evaluated using the MTT assay (Table II). The result demonstrates that a dose-dependent reduction in MTT absorbance for Hela cells incubated with non-conjugated nanoparticles and 2-DG-grafted nanoparticles at all tested concentrations. In all concentration range, they showed little cytotoxic effects to Hela cells and the cells remained more than 80% viable relative to control. And the cytotoxicity of γ-Fe_2O_3-DMSA-DG NPs was lower than that of γ-Fe_2O_3-DMSA NPs. There were no statistically significant differences in the concentration range of 50–600 μg/mL between viability values of the two groups ($p > 0.05$).

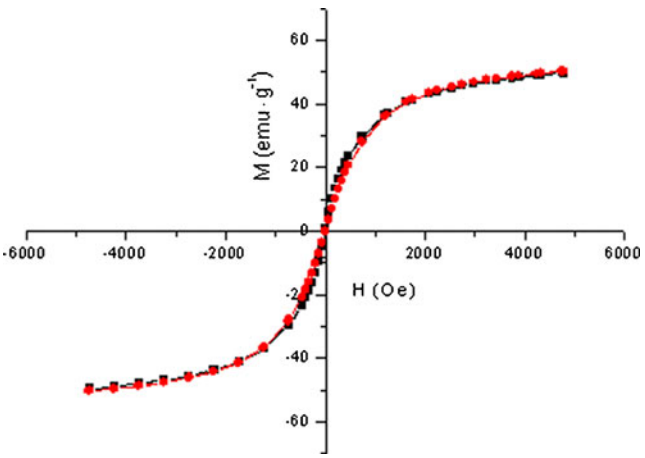

Fig. 5 Hysteresis loops at room temperature for γ-Fe_2O_3-DMSA NPs (*squares*) and γ-Fe_2O_3-DMSA-DG NPs (*circles*). M: magnetization value; H: magnetic field strength.

Cellular Uptake

Cellular uptake of γ-Fe_2O_3-DMSA NPs and γ-Fe_2O_3-DMSA-DG NPs was investigated in Hela cells. To visualize the iron within SPIO NPs labeled cells, Prussian blue staining was performed. Fig. 6 shows the optical micrographs of Prussian blue stained Hela cells after 2 h incubation with 100 μg/mL SPIO NPs. It can be seen that most of the Hela cells incubated with SPIO NPs were stained in blue and no blue spots were observed in the cytoplasm of the control cells without SPIO NPs under the same conditions. And the number of blue spots in Hela cells incubated with γ-Fe_2O_3-DMSA-DG NPs was more than that in the cells incubated with γ-Fe_2O_3-DMSA NPs. Specificity of glucose was also evaluated by competitive binding method. Dependence of SPIO NPs uptake on GLUT family transporters was tested by the addition of the indicated quantities of anti-GLUT1 antibody prior to incubation with SPIO NPs. The results are shown in Fig. 6 (c) and (d). The inhibition phenomena showed exposure of the cells to GLUT1 antibody prior to treatment with 2-DG-grafted NPs significantly eliminated blue spots. Comparatively, non-targeted NPs were not blocked by GLUT1 antibody.

UV colorimetric assay was also utilized to quantify the cellular uptake of γ-Fe_2O_3-DMSA NPs and γ-Fe_2O_3-DMSA-DG NPs into Hela cells in terms of iron concentration. The results shown in Table III demonstrate the specificity of the 2-DG-grafted nanoparticles for the glucose transporter. The uptake of 2-DG-conjuated and non-conjugated nanoparticles by Hela cells was time dependent and increased with time. When the materials were incubated with cells for 4, 8 and 12 h, the 2-DG-grafted nanoparticles showed significant amount of uptake in Hela cells compared to their non-targeted counterparts. Following 4–12 h in culture, the Hela cells incubated with γ-Fe_2O_3-DMSA-DG NPs demonstrated an uptake approximately 1.93–5.25 times higher than the γ-Fe_2O_3-DMSA NPs group with 50–200 μg/mL. This might be due to the high glucose consumption.

MRI

Using a clinical 1.5-T MR scanner, the MRI signal intensity of Hela cells in agarose incubated with SPIO NPs (Fig. 7 (c) and (d)) was significantly decreased (a significant darkening of T_2W signals) compared with water and nonlabeled cells (Fig. 7 (a) and (b)) (no MR contrast). γ-Fe_2O_3-DMSA NPs and γ-Fe_2O_3-DMSA-DG NPs caused noticeable shorter T_2 relaxation times with signal loss in the cells. Mean T_2 relaxation time of γ-Fe_2O_3-DMSA NPs and γ-Fe_2O_3-DMSA-DG NPs internalized Hela cells was 670.6±26.7 and 233.0±

Table II Viability of Labeled Hela Cells Measured at Different Concentrations with MTT Assay

Sample	Concentration (μg/mL)					
	0	50	100	200	400	600
γ-Fe_2O_3-DMSA NPs	100.27 ± 2.40	91.37 ± 9.46	89.63 ± 5.05	85.73 ± 4.90	83.83 ± 8.87	82.07 ± 3.66
γ-Fe_2O_3-DMSA-DG NPs		98.67 ± 5.08	94.80 ± 2.25	91.73 ± 5.88	90.57 ± 4.14	90.83 ± 4.41

9.3 ms, respectively. No changes in T_2 relaxation time were observed in water and nonlabeled cells.

DISCUSSION

Many tumors have been shown to overexpress facilitated glucose transporters. ^{18}F-FDG demonstrates functional imaging at the cellular level, where elevated glucose consumption by malignant cells results in increased uptake of ^{18}F-FDG compared with normal tissue. SPIO NPs hold promise as multifunctional constructs for use in early cancer detection and treatment. If SPIO NPs could be conjugated with glucose analog, a nontoxic tracer for rapid tumor detection, SPIO NPs would potentially be used in various fields of biomedical research, and maybe even clinical applications. In this study, we successfully synthesized 2-deoxy-D-glucose conjugated γ-Fe_2O_3-DMSA NPs by a modified preparation method under very mild conditions without the need of high temperature, organic solvent, surfactant and some other special experimental technology, such as DMSO was commonly used as solvent (31) in this reaction system and was difficult to remove from the solution of SPIO NPs. EDC, as a zero-length crosslinking agent, reacts with carboxyl group of DMSA to form a primary amine-reactive *O*-acylisourea intermediate. In the presence of NHS, EDC can be used to convert carboxyl groups to amine-reactive NHS esters. The bending efficiency was about 40% in our previous paper (data no shown) (19). The process of adding EDC and NHS little by little in the reacting solution reported in this paper could dramatically improve the bending efficien-

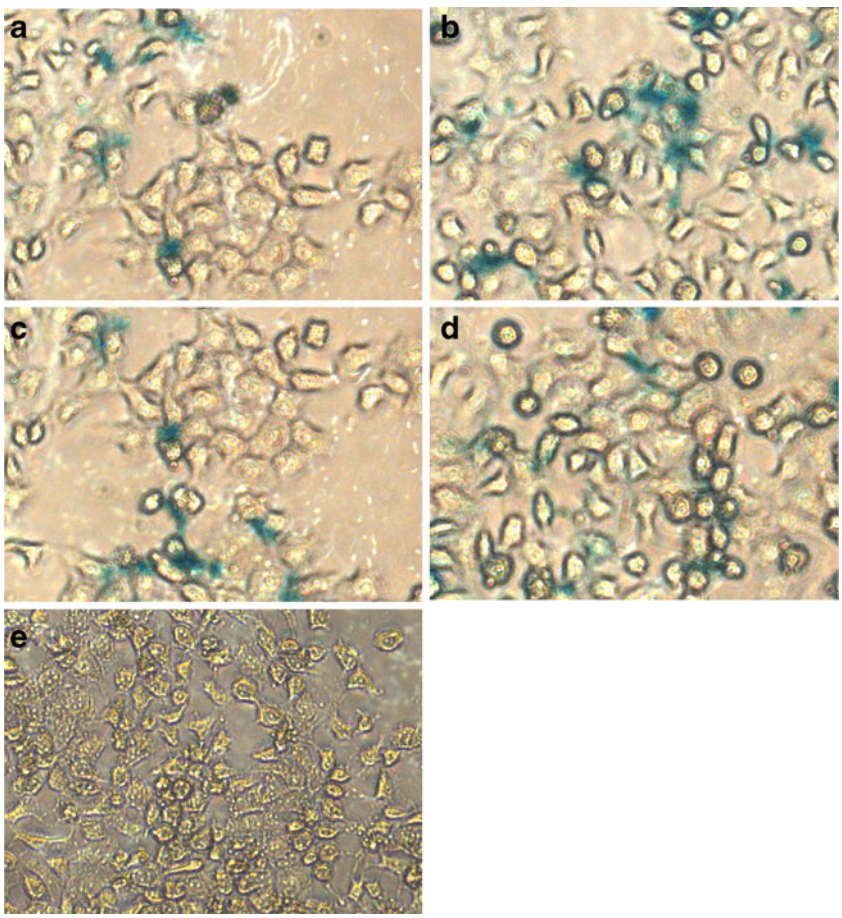

Fig. 6 Prussian blue staining of representative Hela cells labeled with γ-Fe_2O_3-DMSA NPs (**a**), γ-Fe_2O_3-DMSA-DG NPs (**b**), γ-Fe_2O_3-DMSA NPs plus anti GLUT1 antibody (**c**), γ-Fe_2O_3-DMSA-DG NPs plus anti GLUT1 antibody (**d**) and control Hela cells (**e**).

Table III Comparison Uptake of 2-DG-Conjugated γ-Fe_2O_3-DMSA (b) and Non-conjugated γ-Fe_2O_3-DMSA NPs (a) by Hela Cells as Quantified by UV Colorimetric Assay

Conc. of Fe added in the incubation media (μg/mL)	Cellular uptake of Fe per cell (pg)					
	4 h		8 h		12 h	
	a	b	a	b	a	b
50	0.5051 ± 0.0289	2.6521 ± 0.3829	0.5772 ± 0.0626	2.7506 ± 0.1035	0.9043 ± 0.2238	3.8643 ± 0.3109
100	1.7204 ± 0.1055	4.9762 ± 0.5693	2.6007 ± 1.0963	5.0154 ± 0.4629	3.4505 ± 0.0444	6.6851 ± 0.4185
200	3.8176 ± 0.0389	9.4192 ± 1.2322	4.7300 ± 0.1512	9.9460 ± 0.3450	6.0575 ± 0.2805	12.4724 ± 0.2495

cy. This strategy is particularly useful in the present study for conjugation of 2-DG to the surface of nanoparticles through the reaction between carboxylic acid and amino group.

There are no significant difference between the TEM image of γ-Fe_2O_3-DMSA NPs and γ-Fe_2O_3-DMSA-DG NPs. It indicates no further aggregation happened during the conjugation process, which has also been confirmed by hydrodynamic diameter and distribution measurements. FTIR, SEM/EDS and TGA indicate 2-DG is successfully functionalized onto the surface of γ-Fe_2O_3-DMSA NPs. Considering that part of carboxyl groups of DMSA were absorbed on the surface of naked iron oxide particles, free carboxyl groups for further functionalization was limited and unknown. In this paper, the binding efficiency of 2-DG to DMSA coated maghemite nanoparticles was calculated to be about 60% based on total carboxyl groups of DMSA. Therefore, higher binding efficiency could be predicted by our analysis mentioned above.

The majority of cancers and isolated cancer cell lines overexpress the GLUT family members (32,33). In this paper, we chose the research object as Hela cells with high-level surface expression of GLUT1 (34–37). The results of the MTT assay performed in our study indicated that two SPIO NPs had lower cytotoxic effects to Hela cells in a concentration range up to 600 μg/mL as compared with the nonlabeled Hela cells, which could be further explored for biomedical applications. It was surprising that cells incubated with γ-Fe_2O_3-DMSA-DG NPs maintained a higher viability, as it seems like this NPs are promoting growth of tumor cells. Following 4–12 h incubated in cell culture medium of Hela, γ-Fe_2O_3-DMSA-DG NPs showed about 2- to 5-fold higher levels of cellular internalization than γ-Fe_2O_3-DMSA NPs. 2-DG-grafted NPs uptake was also effectively blocked by antibodies against the glucose transport protein GLUT1. Collectively, these results demonstrate specificity of γ-Fe_2O_3-DMSA-DG NPs and suggest involvement of the GLUT family of transporters in its uptake. The results of cellular uptake experiments show the novel targeted magnetic nanoprobes based on higher glucose consumption of tumor cell were successfully designed and prepared.

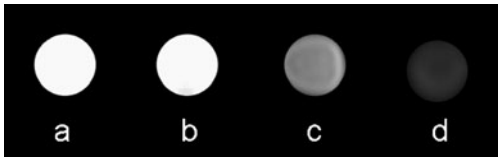

Fig. 7 T_2 weighted MR images of water (**a**), nonlabeled Hela cells (**b**), γ-Fe_2O_3-DMSA NPs-labeled Hela cells (**c**) and γ- Fe_2O_3-DMSA-DG NPs-labeled Hela cells (**d**).

Spin–lattice relaxation time T_1 and spin-spin relaxation time T_2 may be shortened considerably in presence of paramagnetic species. While shortening of T_1 leads to an increase in signal intensity (a bright spot), shortening of T_2 produces broader lines with decreased intensity (a dark spot). The iron oxide-based superparamagnetic is T_2 relaxation-darkening contrast because of their high relaxivities and capacities to achieve T_2. The T_2 relaxation process occurred due to the exchange of energy between protons in water molecules. In the presence of an externally applied magnetic field, inhomogeneity in the magnetic field was created by magnetic nanoparticles which resulted in dephasing of the magnetic moments of protons and hence T_2 shortening. The results of MRI showed that γ-Fe_2O_3-DMSA-DG NPs-labeled Hela cells can be detected *in vitro* with a 1.5T clinical MRI scanner.

According to our preliminary results it becomes obvious that conjugation of 2-DG to γ-Fe_2O_3-DMSA NPs could significantly increase most tumor cells uptake of iron oxide NPs. These novel magnetic nanoparticles may allow separating, diagnosing, monitoring and treating many tumors which have been shown to overexpress facilitated glucose transporters.

CONCLUSION

In this study, we reported a modified preparation and systematically studied the structure, magnetic and other properties of γ-Fe_2O_3-DMSA-DG NPs. 2-DG-grafted nanoparticels showed little cytotoxic effects, significant amount of

uptake in Hela cells and T_2 contrast enhancement compared to their non-targeted counterparts. Therefore, we conclude that 2-DG-grafted γ-Fe_2O_3-DMSA NPs are useful as a multifunctional tumor-targeted SPIO NPs for follow-up applications in the field of magnetic cell separation, MRI, hyperthermia, drug delivery and gene therapy.

ACKNOWLEDGEMENTS & DISCLOSURES

This study was supported by National Basic Research Program of China (No. 2011CB933503), National Natural Science Foundation of China (No. 81001412, 30970754 and 30870689) and China-US International Science and Technology Cooperation Program (2009DFA31990).

REFERENCES

1. Bell GI, Burant CF, Takeda J, Gould GW. Structure and function of mammalian facilitative sugar transporters. J Biol Chem. 1993;268:19161–4.
2. Gold J. Inhibition of Walker 256 intramuscular carcinoma in rats by administration of hydrazine sulfate. Oncology. 1971;25:66–71.
3. Fanciulli M, Valentini A, Bruno T, Citro G, Zupi G, Floridi A. Effect of the antitumor drug lonidamine on glucose metabolism of adriamycin-sensitive and -resistant human breast cancer cells. Oncol Res. 1996;8:111–20.
4. Sokoloff L, Reivich M, Kennedy C, Des Rosiers MH, Patlak CS, Pettigrew KD, *et al.* The [^{14}C]deoxyglucose method for the measurement of local cerebral glucose utilization: theory, procedure, and normal values in the conscious and anesthetized albino rat. J Neurochem. 1977;28:897–916.
5. Turkheimer F, Moresco RM, Lucignani G, Sokoloff L, Fazio F, Schmidt K. The use of spectral analysis to determine regional cerebral glucose utilization with positron emission tomography and [^{18}F]fluorodeoxyglucose: theory, implementation, and optimization procedures. J Cereb Blood Flow Metab. 1994;14:406–22.
6. Dienel GA, Cruz NF, Adachi K, Sokoloff L, Holden JE. Determination of local brain glucose level with [^{14}C]methylglucose: effects of glucose supply and demand. Am J Physiol. 1997;273:E839–49.
7. Axelrod JD, Pilch PF. Unique cytochalasin B binding characteristics of the hepatic glucose carrier. Biochemistry. 1983;22:2222–7.
8. Schmidt KC, Lucignani G, Sokoloff L. Fluorine-18-fluorodeoxyglucose PET to determine regional cerebral glucose utilization: a reexamination. J Nucl Med. 1996;37:394–9.
9. Jin Y, Jia C, Huang SW, O'Donnell M, Gao X. Multifunctional nanoparticles as coupled contrast agents. Nat Commun. 2010;1:41.
10. Liu F, Laurent S, Fattahi H, Elst LV, Muller RN. Superparamagnetic nanosystems based on iron oxide nanoparticles for biomedical imaging. Nanomedicine (Lond). 2011;6:519–28.
11. Fattahi H, Laurent S, Liu F, Arsalani N, Elst LV, Muller RN. Magnetoliposomes as multimodal contrast agents for molecular imaging and cancer nanotheragnostics. Nanomedicine (Lond). 2011;6:529–44.
12. Issadore D, Shao H, Chung J, Newton A, Pittet M, Weissleder R, *et al.* Self-assembled magnetic filter for highly efficient immunomagnetic separation. Lab Chip. 2011;11:147–51.
13. Das M, Dhak P, Gupta S, Mishra D, Maiti TK, Basak A, *et al.* Highly biocompatible and water-dispersible, amine functionalized magnetite nanoparticles, prepared by a low temperature, air-assisted polyol process: a new platform for bio-separation and diagnostics. Nanotechnology. 2010;21:125103.
14. Laurent S, Bridot JL, Elst LV, Muller RN. Magnetic iron oxide nanoparticles for biomedical applications. Future Med Chem. 2010;2:427–49.
15. Yang X, Hong H, Grailer JJ, Rowland IJ, Javadi A, Hurley SA, *et al.* cRGD-functionalized, DOX-conjugated, and ^{64}Cu-labeled superparamagnetic iron oxide nanoparticles for targeted anticancer drug delivery and PET/MR imaging. Biomaterials. 2011;32:4151–60.
16. Yallapu MM, Othman SF, Curtis ET, Gupta BK, Jaggi M, Chauhan SC. Multi-functional magnetic nanoparticles for magnetic resonance imaging and cancer therapy. Biomaterials. 2011;32:1890–905.
17. Elsherbini AA, Saber M, Aggag M, El-Shahawy A, Shokier HA. Magnetic nanoparticle-induced hyperthermia treatment under magnetic resonance imaging. Magn Reson Imaging. 2011;29:272–80.
18. Maity D, Chandrasekharan P, Yang CT, Chuang KH, Shuter B, Xue JM, *et al.* Facile synthesis of water-stable magnetite nanoparticles for clinical MRI and magnetic hyperthermia applications. Nanomedicine (Lond). 2010;5:1571–84.
19. Shan XH, Hu H, Xiong F, Gu N, Geng XD, Zhu W, *et al.* Targeting Glut1-overexpressing MDA-MB-231 cells with 2-deoxy-d-g1ucose modified SPIOs. Eur J Radiol. 2011; [Epub ahead of print] doi:10.1016/j.ejrad.2011.03.013.
20. Molday RS. US Patent 4452773, 1984.
21. Fauconnier N, Pons JN, Roger J, Bee A. Thiolation of maghemite nanoparticles by dimercaptosuccinic acid. J Colloid Interface Sci. 1997;194:427–33.
22. Fauconnier N, Bee A, Roger J, Pons JN. Synthesis of aqueous magnetic liquids by surface complexation of maghemite nanoparticles. J Mol Liq. 1999;83:233–42.
23. Gupta AK, Gupta M. Cytotoxicity suppression and cellular uptake enhancement of surface modified magnetic nanoparticles. Biomaterials. 2005;26:1565–73.
24. Auffan M, Decome L, Rose J, Orsiere T, De Meo M, Briois V, *et al.* *In vitro* interactions between DMSA-coated maghemite nanoparticles and human fibroblasts: a physicochemical and cyto-genotoxical study. Environ Sci Technol. 2006;40:4367–73.
25. Frey NA, Peng S, Cheng K, Sun SH. Magnetic nanoparticles in biomedicine: synthesis, functionalization and applications. Chem Soc Rev. 2009;38:2532–42.
26. Grabis J, Heidemane G, Rašmane D. Preparation of Fe_3O_4 and γ-Fe_2O_3 nanoparticles by liquid and gas phase processes. ISSN 1392–1320 Mater Sci. (Medžlagotyra). 2008;14:292-5.
27. Ge YQ, Zhang S, He SY, Zhang Y, Gu N. Fabrication and characterization of chitosan-poly(acrylic acid) magnetic nanospheres. J Nanoscie Nanotech. 2009;9:1287–90.
28. Nasibulin AG, Shandakov SD, Anisimov AS, Gonzalez D, Jiang H, Pudas M, *et al.* Charging of aerosol products during ferrocene vapor decomposition in N2 and CO atmospheres. J Phys Chem C. 2008;112:5762–9.
29. Zhang S, Zhang Y, Liu JW, Zhang CH, Gu N, Li FQ. Preparation of anti-Sperm protein 17 immunomagnetic nanoparticles for targeting cell. J Nanosci Nanotech. 2008;8:2341–6.
30. Zhang S, Chen SJ, Gu CR, Zhang Y, Xu JD, Bian ZP, Yang D, Gu N. The Effect of iron oxide magnetic nanoparticles on smooth muscle cells. Nanoscale Res Lett. 2009;4:70–7.
31. Sun EY, Josephson L, Kelly KA, Weissleder R. Development of Nanoparticle libraries for biosensing. Bioconjugate Chem. 2006; 17:109–13.

32. Younes M, Lechago LV, Somoano JR, *et al*. Wide expression of the humaneryt hrocyte glucose transporter Glut1 in human cancers. Cancer Res. 1996;56:1164–7.
33. Takata K, Kasahara T, Kasahara M, Ezaki O, Hirano H. Localization of erythrocyte HepG2-type glucose transporter (GLUT1) in human placental villi. Cell Tissue Res. 1992;267:407–12.
34. Jin QW, Agrawal L, VanHorn-Ali Z, Alkhatib G. GLUT-1-independent infection of the glioblastoma/astroglioma U87 cells by the human T cell leukemia virus type 1. Virology. 2006;353:99–110.
35. Zhang W, Cai L, Chen Y, Huang ZW, Yin P. Study on the synthesis o f ^{99}mTc-Gd-DTPA-DG and its up taking by ce rvical cancer cells. Shandong Med J. 2010;50:17–9.
36. Bayly SR, King RC, Honess DJ, Barnard PJ, Betts HM, Holland JP, *et al*. *In vitro* and *in vivo* evaluations of a hydrophilic ^{64}Cu-bis (thiosemicarbazonato)-glucose conjugate for hypoxia imaging. J Nucl Med. 2008;49:1862–8.
37. Ojcius DM, Degani H, Mispelter JM, Dautry-Varsat A. Enhancement of ATP levels and glucose metabolism during an Infection by *Chlamydia*. J Biol Chem. 1998;273:7052–8.